Journal of Sound and Vibration (1997) **207**(1), 15–31

DYNAMIC STIFFNESS ANALYSIS FOR IN-PLANE VIBRATIONS OF ARCHES WITH VARIABLE CURVATURE

Y.-P. TSENG

Department of Civil Engineering, Tamkang University, Tamsui, Taiwan 25137, *R.O.C.*

C. S. HUANG

National Center for Research on Earthquake Engineering, Taipei, Taiwan

AND

C.-J. LIN

Department of Civil Engineering, Tamkang University, Tamsui, Taiwan 25137, *R.O.C.*

(*Received* 10 *January* 1996, *and in final form* 21 *April* 1997)

This paper provides a systematic approach to solve in-plane free vibrations of arches with variable curvature. The proposed approach basically introduces the concept of dynamic stiffness matrix into a series solution for in-plane vibrations of arches with variable curvature. An arch is decomposed into as many elements as needed for accuracy of solution. In each element, a series solution is formulated in terms of polynomials, the coefficients of which are related to each other through recurrence formulas. As a result, in order to have an accurate solution, one does not need a lot of terms in series solution and in Taylor expansion series for the variable coefficients of the governing equations due to the consideration of variable curvature. Finally, a dynamic stiffness matrix is formed such that it can be applied to solve more complicated systems such as multiple-span arches. In the whole analysis, the effects of rotary inertia and shear deformation have been taken into account.

1. INTRODUCTION

Arches are basic structural elements in many practical applications such as bridges, roof structures and aerospace structure. Their importance results in a vast literature published on the dynamic behavior of planar curved structural elements. The review articles [1–3] have summarized much research on this subject. Of this vast literature, some of it deals with the derivation of equations of motion (cf., [4–11]), but most of it principally analyzes free and undamped vibrations. More than 300 articles studying free vibrations of arches are cited in reference [3].

For arches with variable curvature, the Rayleigh–Ritz method has been frequently applied to find the lowest natural frequency of in-plane vibration [12–16]. By following the numerical technique developed by Veletsos *et al*. for a circular arch [9], Lee and Wilson [17] obtained the first three natural frequencies and mode shapes for parabolic, sinusoidal and elliptic arches. Suzuki and his co-workers proposed a series solution in terms of polynomials for the vibration of arches with variable curvature [18–20]. In their solution, the arch is considered as a unit and the formulation of a solution for symmetric modes is separated from that for antisymmetric modes, so that only the problems with symmetry

0022–460X/97/410015 + 17 $25.00/0/sv971112

are studied. There are two main shortcomings in this solution. One is that a convergent solution may not be reached if the convergence radius of the series solution does not cover the whole domain of the arch under consideration. The other is that, in order to obtain accurate results, a lot of terms in Taylor expansion series are needed for those geometric functions related to variable curvature, arc length and their first derivatives. It takes sustained efforts to obtain those Taylor expansion series in formulating the solution.

The main purpose of the present paper is to propose a series solution for vibrations of arches with variable curvature, which improves the solution given by Suzuki and Takahashi [20] by introducing the concept of the dynamic stiffness method. The arch under consideration is decomposed into serveral subdomains (or elements). In each subdomain, a series solution in terms of polynomials is formulated, in which the symmetric solution is not separated from the antisymmetric solution. The series solution satisfies the governing equations, including the effects of shear deformation, axial deformation and rotary inertia. Recursive relations between the coefficients of polynomials are explicitly given. Then, at the ends of the subdomain, the stress resultants (axial force, shear force and moment) are expressed in terms of the displacement components (tangential displacement, normal displacement and rotation due to pure bending) by a so-called local dynamic stiffness matrix. After assembling these local dynamic stiffness matrices for each subdomain through the continuity conditions between subdomains, a global dynamic stiffness matrix can be established, which relates the displacement variables at the nodal points of each element to the external loading. Finally, one can solve for the natural frequencies by substituting the boundary conditions into the relations between the nodal displacements and external loading. A similar philosophy was applied by Leung and Zhou [21] to solve for vibrations of non-uniform Timoshenko beams.

To demonstrate the validity of the proposed solution as well as to investigate the characteristics of the proposed method, a convergence study is carried out for the vibration of a circular arch. Finally, the proposed method is applied to obtain the first six natural frequencies of parabolic and elliptic arches having uniform rectangular cross-sections with various boundary conditions and geometry parameters. The geometry parameters considered here are the ratio of rise to span length, h/l, and the ratio of span length to radius of gyration of cross-section area, l/γ, for parabolic arches; opening angle, θ_0, the ratio of long-axis length to short-axis length, a/b, and the ratio of twice long-axis length to radius of gyration of cross-section area, $2a/\gamma$, for elliptic arches. Numerical results are presented for $h/l = 0{\cdot}2$, $0{\cdot}4$, $0{\cdot}6$ and $0{\cdot}8$, and $l/\gamma = 10$ and 100 for parabolic arches. In the cases for elliptic arches, θ_0 is set equal to 60°, 120° and 180°; a/b is set equal to $0{\cdot}2$, $0{\cdot}5$ and $0{\cdot}8$; and $2a/\gamma$ is set equal to 10 and 100.

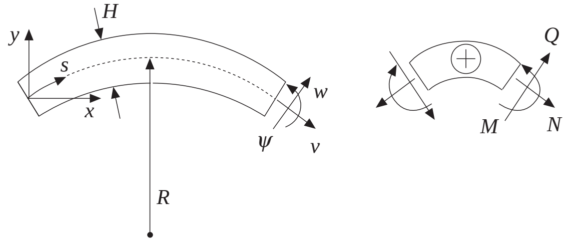

Figure 1. The defining sketch for an arch.

2. GOVERNING EQUATIONS

Shown in Figure 1 is an arch of thickness H with radius R of the centroidal axis that is a function of S, the arc length of centroidal axis measured from the left support. The tangential and radial displacements of the centroidal axis are denoted by v and w, respectively, while ψ represents the rotation of the centroidal axis due to bending only. The sign convention for positive displacements, moment (M), shear force (Q) and axial force (N) is also given in Figure 1. The equations of motion obtained from dynamic equilibrium if there is no external loading are (cf., Chidamparam and Leissa [3])

$$\frac{\partial N}{\partial S}+\frac{Q}{R}=\rho A\ddot{v}, \qquad \frac{\partial Q}{\partial S}-\frac{N}{R}=\rho A\ddot{w}, \qquad \frac{\partial M}{\partial S}+Q=\rho I\ddot{\psi}, \tag{1}$$

where ρ is the mass per unit volume, A is the area of the cross-section, I is the second moment of the area of cross-section, and the derivative with respect to time is denoted by a dot. Assuming a linearly elastic material, the relations between the displacement and rotation components and the stress resultants are (cf., Chidamparam and Leissa [3])

$$N=EA\left(\frac{\partial v}{\partial S}+\frac{w}{R}\right), \qquad Q=\kappa AG\left(\frac{\partial w}{\partial S}-\frac{v}{R}-\psi\right), \qquad M=EI\frac{\partial \psi}{\partial S}, \tag{2a–c}$$

where κ is the shear coefficient of the cross-section. In equations (1) and (2), it is noted that the effects of axial deformation, shear deformation and rotary inertia are considered.

Then, substituting equations (2) into equations (1) and assuming a uniform cross-section and constant material properties through the arch yields

$$EA\frac{\partial^2 v}{\partial S^2}-\frac{\kappa GA}{R^2}v-\frac{\kappa GA}{R}\psi+\frac{A(E+\kappa G)}{R}\frac{\partial w}{\partial S}+EAw\frac{\partial}{\partial S}\left(\frac{1}{R}\right)=\rho A\ddot{v}, \tag{3a}$$

$$\kappa AG\frac{\partial^2 w}{\partial S^2}-\frac{EA}{R^2}w-\kappa GA\frac{\partial \psi}{\partial S}-\frac{A(E+\kappa G)}{R}\frac{\partial v}{\partial S}-\kappa GAv\frac{\partial}{\partial S}\left(\frac{1}{R}\right)=\rho A\ddot{w}, \tag{3b}$$

$$EI\frac{\partial^2 \psi}{\partial S^2}-\kappa GA\psi-\frac{\kappa AG}{R}v+\kappa GA\frac{\partial w}{\partial S}=\rho I\ddot{\psi}, \tag{3c}$$

where the dots denote time derivatives. Equations (3) are the governing equations for in-plane free vibrations of arches with variable curvature.

It should be noted that it is usually complicated to express the curvature as a function of S. For a typical arch geometry such as a parabola, it is simple to express the curvature as a function of the Cartesian co-ordinate, x (see Figure 1). Therefore, in the following formulation of solution, we transform the co-ordinates S to x. Furthermore, it is convenient to introduce a representative length of the arch under consideration, L, such that one can define the following dimensionless quantities:

$$\bar{x}=x/L, \qquad \bar{y}=y/L, \qquad \bar{w}=w/L, \qquad \bar{v}=v/L, \qquad \overline{S}=S/L, \qquad \overline{R}=R/L. \tag{4}$$

Then, equations (3) can be expressed as follows, after some arrangement:

$$\bar{v}''+\bar{v}'\frac{\xi'}{\xi}-\frac{\lambda^2}{\xi^2\overline{R}^2}\bar{v}-\frac{\lambda^2}{\xi^2\overline{R}}\psi+\frac{1+\lambda^2}{\xi\overline{R}}\bar{w}'-\frac{\overline{R}'}{\xi\overline{R}^2}\bar{w}=\frac{\rho L^2}{E\xi^2}\ddot{\bar{v}}, \tag{5a}$$

$$\bar{w}'' + \frac{\xi'}{\xi}\bar{w}' - \frac{1}{\lambda^2\xi^2\bar{R}^2}\bar{w} - \frac{1}{\xi}\psi' - \frac{1+\lambda^2}{\lambda^2\xi\bar{R}}\bar{v}' + \frac{\bar{R}'}{\xi\bar{R}^2}\bar{v} = \frac{\rho L^2}{E\xi^2}\frac{1}{\lambda^2}\ddot{\bar{w}}, \tag{5b}$$

$$\psi'' + \frac{\xi'}{\xi}\psi' - \frac{\lambda^2}{\xi^2\bar{\gamma}^2}\psi + \frac{\lambda^2}{\xi\bar{\gamma}^2}\bar{w}' - \frac{\lambda^2}{\xi^2\bar{\gamma}^2\bar{R}}\bar{v} = \frac{\rho L^2}{E\xi^2}\ddot{\psi}, \tag{5c}$$

where the primes denote derivatives with respect to $\bar{x}$, and $\xi = \mathrm{d}x/\mathrm{d}S = \mathrm{d}\bar{x}/\mathrm{d}\bar{S}$, $\lambda^2 = \kappa G/E$ and $\bar{\gamma}^2 = I/(L^2 A)$.

3. METHOD OF SOLUTION

To solve free vibration problems, one can assume that the solution form for equations (5) can be expressed as follows:

$$\bar{v}(\bar{x}, t) = \bar{V}(\bar{x})\,\mathrm{e}^{\mathrm{i}\omega t}, \qquad \bar{w}(\bar{x}, t) = \bar{W}(\bar{x})\,\mathrm{e}^{\mathrm{i}\omega t}, \qquad \psi(\bar{x}, t) = \Psi(\bar{x})\,\mathrm{e}^{\mathrm{i}\omega t}. \tag{6}$$

Accordingly, the solutions for the stress resultants are given in the following form:

$$N(\bar{x}, t) = \bar{N}(\bar{x})\,\mathrm{e}^{\mathrm{i}\omega t}, \qquad Q(\bar{x}, t) = \bar{Q}(\bar{x})\,\mathrm{e}^{\mathrm{i}\omega t}, \qquad M(\bar{x}, t) = \bar{M}(\bar{x})\,\mathrm{e}^{\mathrm{i}\omega t}. \tag{7}$$

Substitution of equations (6) into equations (5) and careful rearrangement result in

$$\bar{V}'' + \bar{V}'\frac{\xi'}{\xi} - \frac{\lambda^2}{\xi^2\bar{R}^2}\bar{V} - \frac{\lambda^2}{\xi^2\bar{R}}\Psi + \frac{1+\lambda^2}{\xi\bar{R}}\bar{W}' - \frac{\bar{R}'}{\xi\bar{R}^2}\bar{W} = -\frac{\rho L^2}{E\xi^2}\omega^2\bar{V}, \tag{8a}$$

$$\bar{W}'' + \frac{\xi'}{\xi}\bar{W}' - \frac{1}{\lambda^2\xi^2\bar{R}^2}\bar{W} - \frac{1}{\xi}\Psi' - \frac{1+\lambda^2}{\lambda^2\xi\bar{R}}\bar{V}' + \frac{\bar{R}'}{\xi\bar{R}^2}\bar{V} = -\frac{\rho L^2}{E\xi^2}\frac{\omega^2}{\lambda^2}\bar{W}, \tag{8b}$$

$$\Psi'' + \frac{\xi'}{\xi}\Psi' - \frac{\lambda^2}{\xi^2\bar{\gamma}^2}\Psi + \frac{\lambda^2}{\xi\bar{\gamma}^2}\bar{W}' - \frac{\lambda^2}{\xi^2\bar{\gamma}^2\bar{R}}\bar{V} = -\frac{\rho L^2}{E\xi^2}\omega^2\Psi. \tag{8c}$$

Equations (8) are a set of second order ordinary differential equations for $\bar{V}$, $\bar{W}$ and Ψ with coefficients that are functions of one independent variable, $\bar{x}$, only.

The Frobenius method [22] can be applied to solve equations (8). At first, for convenience, we express the following functions by their Taylor expansion series about a point on the arch under consideration with the non-dimensional position co-ordinates, η:

$$\frac{\xi'}{\xi} = \sum_{k=0}^{K} a_k\,(\bar{x}-\eta)^k, \qquad \frac{1}{\xi^2} = \sum_{k=0}^{K} b_k\,(\bar{x}-\eta)^k, \qquad \frac{1}{\xi^2\bar{R}} = \sum_{k=0}^{K} c_k\,(\bar{x}-\eta)^k,$$

$$\frac{\bar{R}'}{\xi\bar{R}^2} = \sum_{k=0}^{K} d_k\,(\bar{x}-\eta)^k, \qquad \frac{1}{\xi} = \sum_{k=0}^{K} e_k\,(\bar{x}-\eta)^k, \qquad \frac{1}{\xi^2\bar{R}^2} = \sum_{k=0}^{K} f_k\,(\bar{x}-\eta)^k,$$

$$\frac{1}{\xi\bar{R}} = \sum_{k=0}^{K} g_k\,(\bar{x}-\eta)^k. \tag{9}$$

It is worth mentioning that some of the expressions in equations (9) are correlated with each other. For example, $b_J = \Sigma_{k=0}^{J} e_{J-k}\,e_k$. However, to make the formulation of the solution simple and clear, as given in the following, it would be better to leave the expressions in equations (9) the way they are. The coefficients, a_k, b_k, ..., g_k can be determined if the geometry of the arch of interests is defined. Consequently, it is reasonable and straightforward to express the solution of equations (8) in terms of polynomials such as

$$\bar{V} = \sum_{j=0}^{J} A_j\,(\bar{x} - \eta)^j, \qquad \bar{W} = \sum_{j=0}^{J} B_j\,(\bar{x} - \eta)^j, \qquad \Psi = \sum_{j=0}^{J} D_j\,(\bar{x} - \eta)^j. \tag{10}$$

Theoretically, J should approach infinity. However, it only needs a finite number of terms in equations (10) to obtain accurate results.

Substituting equations (9) and (10) into equations (8) with very careful rearrangement yields

$$\sum_{j=0}^{J} \Bigg\{ (j+2)\,(j+1)A_{j+2} + \sum_{k=0}^{j} \Bigg[(k+1)a_{j-k}\,A_{k+1} + (1+\lambda^2)\,(k+1)g_{j-k}\,B_{k+1}$$

$$+ \left(\frac{\rho}{E}\,\omega^2 L^2 b_{j-k} - \lambda^2 f_{j-k} \right) A_k - d_{j-k}\,B_k - \lambda^2 c_{j-k}\,D_k \Bigg] \Bigg\} (\bar{x} - \eta)^j = 0, \tag{11a}$$

$$\sum_{j=0}^{J} \Bigg\{ (j+2)\,(j+1)B_{j+2} + \sum_{k=0}^{j} \Bigg[-(k+1)\,\frac{1+\lambda^2}{\lambda^2}\,g_{j-k}\,A_{k+1} + (k+1)a_{j-k}\,B_{k+1}$$

$$-\,(k+1)e_{j-k}\,D_{k+1} + d_{j-k}\,A_k + \left(\frac{\rho}{E}\,\frac{\omega^2 L^2}{\lambda^2}\,b_{j-k} - \frac{1}{\lambda^2} f_{j-k} \right) B_k \Bigg] \Bigg\} (\bar{x} - \eta)^j = 0, \tag{11b}$$

$$\sum_{j=0}^{J} \Bigg\{ (j+2)\,(j+1)D_{j+2} + \sum_{k=0}^{j} \Bigg[(k+1)\,\frac{\lambda^2}{\bar{\gamma}^2}\,e_{j-k}\,B_{k+1} + (k+1)a_{j-k}\,D_{k+1}$$

$$- \frac{\lambda^2}{\bar{\gamma}^2}\,c_{j-k}\,A_k + \left(\frac{\rho}{E}\,\omega^2 L^2 - \frac{\lambda^2}{\bar{\gamma}^2} \right) b_{j-k} D_k \Bigg] \Bigg\} (\bar{x} - \eta)^j = 0. \tag{11c}$$

To satisfy equations (11) for all $\bar{x}$ yields that the coefficients of each order of polynomials have to be zero. Consequently, one obtains the following recursive equations for the coefficients of polynomials in equations (10):

$$A_{j+2} = \frac{-1}{(j+1)\,(j+2)} \Bigg\{ \sum_{k=0}^{j} \Bigg[(k+1)a_{j-k}\,A_{k+1} + (1+\lambda^2)\,(k+1)g_{j-k}\,B_{k+1}$$

$$+ \left(\frac{\rho}{E}\,\omega^2 L^2 b_{j-k} - \lambda^2 f_{j-k} \right) A_k - d_{j-k}\,B_k - \lambda^2 c_{j-k}\,D_k \Bigg] \Bigg\}, \tag{12a}$$

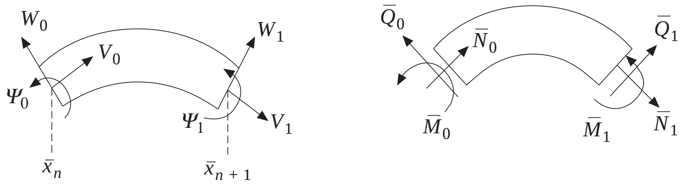

Figure 2. Positive displacements, forces and moments for the nth element, with the common factor $e^{i\omega t}$ omitted.

$$B_{j+2} = \frac{-1}{(j+1)(j+2)} \left\{ \sum_{k=0}^{j} \left[-(k+1)\frac{1+\lambda^2}{\lambda^2} g_{j-k} A_{k+1} + (k+1) a_{j-k} B_{k+1} \right.\right.$$

$$\left.\left. -(k+1) e_{j-k} D_{k+1} + d_{j-k} A_k + \left(\frac{\rho}{E} \frac{\omega^2 L^2}{\lambda^2} b_{j-k} - \frac{1}{\lambda^2} f_{j-k} \right) B_k \right] \right\}, \tag{12b}$$

$$D_{j+2} = -\frac{1}{(j+1)(j+2)} \left\{ \sum_{k=0}^{j} \left[(k+1)\frac{\lambda^2}{\bar{\gamma}^2} e_{j-k} B_{k+1} + (k+1) a_{j-k} D_{k+1} \right.\right.$$

$$\left.\left. -\frac{\lambda^2}{\bar{\gamma}^2} c_{j-k} A_k + \left(\frac{\rho}{E} \omega^2 L^2 - \frac{\lambda^2}{\bar{\gamma}^2} \right) b_{j-k} D_k \right] \right\}, \tag{12c}$$

where $j = 0, 1, 2, \ldots$. From equations (12), A_{j+2}, B_{j+2} and D_{j+2} can be determined if A_0, A_1, B_0, B_1, D_0 and D_1 are known. As a result, the solution of equations (8) can be simply represented as

$$\bar{V}(\bar{x}) = A_0 \bar{v}_0(\bar{x}) + A_1 \bar{v}_1(\bar{x}) + B_0 \bar{v}_2(\bar{x}) + B_1 \bar{v}_3(\bar{x}) + D_0 \bar{v}_4(\bar{x}) + D_1 \bar{v}_5(\bar{x}), \tag{13a}$$

$$\bar{W}(\bar{x}) = A_0 \bar{w}_0(\bar{x}) + A_1 \bar{w}_1(\bar{x}) + B_0 \bar{w}_2(\bar{x}) + B_1 \bar{w}_3(\bar{x}) + D_0 \bar{w}_4(\bar{x}) + D_1 \bar{w}_5(\bar{x}), \tag{13b}$$

$$\Psi(\bar{x}) = A_0 \psi_0(\bar{x}) + A_1 \psi_1(\bar{x}) + B_0 \psi_2(\bar{x}) + B_1 \psi_3(\bar{x}) + D_0 \psi_4(\bar{x}) + D_1 \psi_5(\bar{x}), \tag{13c}$$

where $\bar{v}_j$, $\bar{w}_j$ and ψ_j $(j = 0, 1, 2, \ldots, 5)$ are polynomials the coefficients of which are determined from equations (12).

Up to this point, one can determine the coefficients A_0, A_1, B_0, B_1, D_0, and D_1 from the boundary conditions of the problem of interest. However, by doing this, one can expect that sufficiently large K and J in equations (9) and (10), respectively, are required to result in accurate solutions. It is the most troublesome part in the above solution procedure in finding the coefficients in equations (9), even though one can accomplish this task through the aid of commercial symbolic logic computer packages such as Mathematica™ or MACSYMA™. Besides, one may face the convergence problem of the solution given in equation (10) if the convergence radius could not cover the whole range of $\bar{x}$ under consideration.

To overcome these difficulties, the concept of dynamic stiffness method is introduced into the series solution. The arch under consideration is decomposed into several elements (or subdomains). For each element (see Figure 2), one can construct the following relation from equations (13):

$$\begin{Bmatrix} \bar{V}_0 \\ \bar{W}_0 \\ \Psi_0 \\ \bar{V}_1 \\ \bar{W}_1 \\ \Psi_1 \end{Bmatrix}_n$$

$$= \begin{bmatrix} \bar{v}_0(\bar{x}_n) & \bar{v}_1(\bar{x}_n) & \bar{v}_2(\bar{x}_n) & \bar{v}_3(\bar{x}_n) & \bar{v}_4(\bar{x}_n) & \bar{v}_5(\bar{x}_n) \\ \bar{w}_0(\bar{x}_n) & \bar{w}_1(\bar{x}_n) & \bar{w}_2(\bar{x}_n) & \bar{w}_3(\bar{x}_n) & \bar{w}_4(\bar{x}_n) & \bar{w}_5(\bar{x}_n) \\ \psi_0(\bar{x}_n) & \psi_1(\bar{x}_n) & \psi_2(\bar{x}_n) & \psi_3(\bar{x}_n) & \psi_4(\bar{x}_n) & \psi_5(\bar{x}_n) \\ \bar{v}_0(\bar{x}_{n+1}) & \bar{v}_1(\bar{x}_{n+1}) & \bar{v}_2(\bar{x}_{n+1}) & \bar{v}_3(\bar{x}_{n+1}) & \bar{v}_4(\bar{x}_{n+1}) & \bar{v}_5(\bar{x}_{n+1}) \\ \bar{w}_0(\bar{x}_{n+1}) & \bar{w}_1(\bar{x}_{n+1}) & \bar{w}_2(\bar{x}_{n+1}) & \bar{w}_3(\bar{x}_{n+1}) & \bar{w}_4(\bar{x}_{n+1}) & \bar{w}_5(\bar{x}_{n+1}) \\ \psi_0(\bar{x}_{n+1}) & \psi_1(\bar{x}_{n+1}) & \psi_2(\bar{x}_{n+1}) & \psi_3(\bar{x}_{n+1}) & \psi_4(\bar{x}_{n+1}) & \psi_5(\bar{x}_{n+1}) \end{bmatrix}_n \begin{Bmatrix} A_0 \\ A_1 \\ B_0 \\ B_1 \\ D_0 \\ D_1 \end{Bmatrix}_n$$

$$= [\beta]_n \begin{Bmatrix} A_0 \\ A_1 \\ B_0 \\ B_1 \\ D_0 \\ D_1 \end{Bmatrix}_n, \tag{14}$$

where the subscript n for vectors and the matrix represents the results for the nth element. The components of the vector on the left side of equation (14) are the amplitudes of the nodal displacements and bending rotation of the nth element. For the nth element, η implicit in equation (14) is set equal to $(\bar{x}_n + \bar{x}_{n+1})/2$.

From the displacement–force relationships given in equations (2) after transforming the independent variable S to x and using equations (4) and (14), one can obtain the following expression for the magnitude of stress resultants of the nodal points for the nth element of an arch under vibration in terms of the unknown coefficients (see Figure 2):

$$\begin{Bmatrix} \bar{N}_0 \\ \bar{Q}_0 \\ \bar{M}_0 \\ \bar{N}_1 \\ \bar{Q}_1 \\ \bar{M}_1 \end{Bmatrix}_n = (EA)_n \left([\alpha_1]_n + [\alpha_2]_n + [\alpha_3]_n\right) \begin{Bmatrix} A_0 \\ A_1 \\ B_0 \\ B_1 \\ D_0 \\ D_1 \end{Bmatrix}_n, \tag{15}$$

where

$$[\alpha_1]_n = \begin{bmatrix} -\xi(\bar{x}_n) & 0 & 0 & 0 & 0 & 0 \\ 0 & -\lambda^2\xi(\bar{x}_n) & 0 & 0 & 0 & 0 \\ 0 & 0 & -\bar{\gamma}^2 L\xi(\bar{x}_n) & 0 & 0 & 0 \\ 0 & 0 & 0 & \xi(\bar{x}_{n+1}) & 0 & 0 \\ 0 & 0 & 0 & 0 & \lambda^2\xi(\bar{x}_{n+1}) & 0 \\ 0 & 0 & 0 & 0 & 0 & \bar{\gamma}^2 L\xi(\bar{x}_{n+1}) \end{bmatrix}$$

$$\times \begin{bmatrix} \bar{v}_0'(\bar{x}_n) & \bar{v}_1'(\bar{x}_n) & \bar{v}_2'(\bar{x}_n) & \bar{v}_3'(\bar{x}_n) & \bar{v}_4'(\bar{x}_n) & \bar{v}_5'(\bar{x}_n) \\ \bar{w}_0'(\bar{x}_n) & \bar{w}_1'(\bar{x}_n) & \bar{w}_2'(\bar{x}_n) & \bar{w}_3'(\bar{x}_n) & \bar{w}_4'(\bar{x}_n) & \bar{w}_5'(\bar{x}_n) \\ \psi_0'(\bar{x}_n) & \psi_1'(\bar{x}_n) & \psi_2'(\bar{x}_n) & \psi_3'(\bar{x}_n) & \psi_4'(\bar{x}_n) & \psi_5'(\bar{x}_n) \\ \bar{v}_0'(\bar{x}_{n+1}) & \bar{v}_1'(\bar{x}_{n+1}) & \bar{v}_2'(\bar{x}_{n+1}) & \bar{v}_3'(\bar{x}_{n+1}) & \bar{v}_4'(\bar{x}_{n+1}) & \bar{v}_5'(\bar{x}_{n+1}) \\ \bar{w}_0'(\bar{x}_{n+1}) & \bar{w}_1'(\bar{x}_{n+1}) & \bar{w}_2'(\bar{x}_{n+1}) & \bar{w}_3'(\bar{x}_{n+1}) & \bar{w}_4'(\bar{x}_{n+1}) & \bar{w}_5'(\bar{x}_{n+1}) \\ \psi_0'(\bar{x}_{n+1}) & \psi_1'(\bar{x}_{n+1}) & \psi_2'(\bar{x}_{n+1}) & \psi_3'(\bar{x}_{n+1}) & \psi_4'(\bar{x}_{n+1}) & \psi_5'(\bar{x}_{n+1}) \end{bmatrix}, \tag{16a}$$

$$[\alpha_2]_n = \begin{bmatrix} -\dfrac{1}{\bar{R}(\bar{x}_n)} & 0 & 0 & 0 & 0 & 0 \\ 0 & \dfrac{\lambda^2}{\bar{R}(\bar{x}_n)} & 0 & 0 & 0 & 0 \\ 0 & 0 & 0 & 0 & 0 & 0 \\ 0 & 0 & 0 & \dfrac{1}{\bar{R}(\bar{x}_{n+1})} & 0 & 0 \\ 0 & 0 & 0 & 0 & -\dfrac{\lambda^2}{\bar{R}(\bar{x}_{n+1})} & 0 \\ 0 & 0 & 0 & 0 & 0 & 0 \end{bmatrix}$$

$$\times \begin{bmatrix} \bar{w}_0(\bar{x}_n) & \bar{w}_1(\bar{x}_n) & \bar{w}_2(\bar{x}_n) & \bar{w}_3(\bar{x}_n) & \bar{w}_4(\bar{x}_n) & \bar{w}_5(\bar{x}_n) \\ \bar{v}_0(\bar{x}_n) & \bar{v}_1(\bar{x}_n) & \bar{v}_2(\bar{x}_n) & \bar{v}_3(\bar{x}_n) & \bar{v}_4(\bar{x}_n) & \bar{v}_5(\bar{x}_n) \\ 0 & 0 & 0 & 0 & 0 & 0 \\ \bar{w}_0(\bar{x}_{n+1}) & \bar{w}_1(\bar{x}_{n+1}) & \bar{w}_2(\bar{x}_{n+1}) & \bar{w}_3(\bar{x}_{n+1}) & \bar{w}_4(\bar{x}_{n+1}) & \bar{w}_5(\bar{x}_{n+1}) \\ \bar{v}_0(\bar{x}_{n+1}) & \bar{v}_1(\bar{x}_{n+1}) & \bar{v}_2(\bar{x}_{n+1}) & \bar{v}_3(\bar{x}_{n+1}) & \bar{v}_4(\bar{x}_{n+1}) & \bar{v}_5(\bar{x}_{n+1}) \\ 0 & 0 & 0 & 0 & 0 & 0 \end{bmatrix}, \tag{16b}$$

$$[\alpha_3]_n = \lambda^2 \begin{bmatrix} 0 & 0 & 0 & 0 & 0 & 0 \\ \psi_0(\bar{x}_n) & \psi_1(\bar{x}_n) & \psi_2(\bar{x}_n) & \psi_3(\bar{x}_n) & \psi_4(\bar{x}_n) & \psi_5(\bar{x}_n) \\ 0 & 0 & 0 & 0 & 0 & 0 \\ 0 & 0 & 0 & 0 & 0 & 0 \\ -\psi_0(\bar{x}_{n+1}) & -\psi_1(\bar{x}_{n+1}) & -\psi_2(\bar{x}_{n+1}) & -\psi_3(\bar{x}_{n+1}) & -\psi_4(\bar{x}_{n+1}) & -\psi_5(\bar{x}_{n+1}) \\ 0 & 0 & 0 & 0 & 0 & 0 \end{bmatrix}. \tag{16c}$$

From equations (14) and (15), one can find that

$$\begin{Bmatrix} \bar{N}_0 \\ \bar{Q}_0 \\ \bar{M}_0 \\ \bar{N}_1 \\ \bar{Q}_1 \\ \bar{M}_1 \end{Bmatrix}_n = [\tilde{K}]_n \begin{Bmatrix} \bar{V}_0 \\ \bar{W}_0 \\ \Psi_0 \\ \bar{V}_1 \\ \bar{W}_1 \\ \Psi_1 \end{Bmatrix}_n, \tag{17}$$

where the local dynamic stiffness matrix for the nth element is

$$[\tilde{K}]_n = (EA)_n\,([\alpha_1]_n + [\alpha_2]_n + [\alpha_3]_n)\,[\beta]_n^{-1}. \tag{18}$$

From the continuity conditions between adjacent elements, one can assemble the local dynamic stiffness matrices for each element and obtain the global dynamic stiffness matrix, $[\tilde{K}]$, such that

$$[\tilde{K}]\{U\} = \{F\}, \tag{19}$$

where $\{U\}$ is the vector for the magnitude of nodal displacements of an arch under vibration, while $\{F\}$ is the vector for the magnitude of loading applied at the nodal points.

To compute the natural frequencies of an arch, one has to substitute the geometry boundary conditions into equation (19) and leave out the rows and columns of $[\tilde{K}]$ associated with the geometry boundary conditions. Let the resultant dynamic stiffness matrix be denoted by $[\tilde{K}]_{sub}$. Accordingly, one has

$$[\tilde{K}]_{sub}\,\{U\}_{sub} = \{0\}, \tag{20}$$

where $\{U\}_{sub}$ is the unknown nodal displacement vector which is a subvector of $\{U\}$ by leaving out the nodal displacements (including bending rotation component) described in the boundary conditions. The natural frequencies are the roots making the determinant of $[\tilde{K}]_{sub}$ equal to zero.

Subroutine "DZREAL" in the IMSL (International Mathematical and Statistical Library), which uses Müller's method [23], was applied to find the natural frequencies. The subroutine locates a real value of ω resulting in the determinant of $[\tilde{K}]_{sub}$ equal to zero through an iteration process, starting with an initial guess. An initial guess can be chosen from a roughly determined interval in which the determinant changes sign.

To find the mode shapes, one can compute the eigenvectors corresponding to each natural frequencies from equation (20). Then, one can calculate the functions describing the corresponding mode shapes in each element from equations (13) and (14).

4. CONVERGENCE STUDY

The accuracy of the solution given in the previous section is dependent on K in equation (8), J in equation (9) and the number of elements. $(K+1)$ in equation (8) denotes the number of expansion terms for describing the geometry properties of the arch under consideration in each element, while J in equation (9) denotes the highest order of polynomial used in the solution for each element. To show the validity of the proposed approach and the effects of K, J and the number of elements on the solution, a convergence study was carried out for a uniform circular fixed–fixed arch with $h/R = 0{\cdot}01$ and an opening angle equal to 100°. There is an analytical exact solution for this problem. It should be mentioned that the Poisson ratio is equal to 0·3 for all the numerical results shown in the paper.

In Tables 1–3 are listed the first six non-dimensional natural frequencies, $\omega R^2\sqrt{\rho A/EI}$, by using four, eight and 16 elements with different combinations of J and K, respectively. In these tables, two sets of exact solutions are given. The set denoted by Huang was obtained by the second author following the procedure given by Wang and Guilbert [24]. These two sets of exact solutions differ slightly and the reason is that results given by Chidamparam and Leissa [25] were obtained from the governing equations without shear deformation. The results for $(K+1) = 25$ and $(J+1) = 80$ in Table 1 are very close to the exact solutions, while the results given in Tables 2 and 3 show that one can obtain improved solutions, as expected, by increasing the number of elements and using smaller values for K and J. A comparison of the results obtained from the proposed approach with the exact solution reveals that there are two ways to judge whether the results converge to the solutions with required accuracy. For the fixed number of elements, convergent solutions are obtained if the results do not change by increasing K and J at the same time. For example, the solutions for $K = 9$ and $J = 19$ in Table 3 are the desired convergent results. On the other hand, for the fixed K and J, convergent solutions are obtained if the results do not change by increasing the number of elements. For example, the results for $K = 14$ and $J = 19$ in Table 2 are convergent to six significant figures. It is not necessarily true that the results for the first mode obtained from the proposed approach will converge faster to the exact one than those for other modes as in most of the approximation methods, e.g. the Ritz method and the finite element method.

It is interesting to observe from Tables 1–3 that if the value for K is not large enough, one will obtain results that are convergent to a wrong answer by increasing J only. These convergent results are the solutions for the arch having a slightly different geometry from that under consideration because the series expressions given in equation (9) do not precisely and uniformly converge to the real geometry functions.

As regards this point, there is no doubt that the proposed method can provide very accurate solutions. However, one may wonder how much computational effort is required. By comparing the computational time with a commercial finite element package (SAP90) in solving the same problem, we found that whether or not the proposed approach is superior to a finite element solution depends on the required accuracy of the numerical results. For example, to reach convergent results with six significant figures for the first six modes, SAP90 took 69·04 s for the results with 2048 beam elements, while the present method only needed 40·04 s to obtain the solutions with $K = 14$ and $J = 19$ for each of eight elements shown in Table 3 through six iterations in the subroutine "DZREAL" for

TABLE 1

Convergence of frequency parameters $\omega R^2\sqrt{\rho A/EI}$ for a fixed–fixed circular arch by using four elements

Modes	$(K+1)$ in equations (8)	$(J+1)$ in equations (9)			Exact	
		20	40	80	C&L*	Huang
1	10	18·2423	17·9134	17·9134	17·9249	17·9156
	15	17·9699	17·9155	17·9155		
	25	17·9136	17·9158	17·9158		
2	10	34·8724	34·6048	34·6049	34·6752	34·6428
	15	34·6453	34·6432	34·6432		
	25	34·6404	34·6428	34·6428		
3	10	62·7783	62·6581	62·6582	62·8782	62·7886
	15	62·7777	62·7902	62·7902		
	25	62·7869	62·7887	62·7887		
4	10	92·2484	92·5468	92·5468	92·8664	92·6767
	15	92·7778	92·6781	92·6781		
	25	92·6889	92·6767	92·6767		
5	10	133·569	133·591	133·591	/	133·613
	15	133·704	133·613	133·613		
	25	133·631	133·613	133·613		
6	10	175·795	175·594	175·594	/	175·602
	15	175·757	175·602	175·602		
	25	175·641	175·602	175·602		

*Data from Chidamparam and Leissa [25].
"/" indicates that no data is available.

TABLE 2

Convergence of frequency parameters $\omega R^2\sqrt{\rho A/EI}$ for a fixed–fixed circular arch by using eight elements

Modes	$(K+1)$ in equations (8)	$(J+1)$ in equations (9): 10	20	40	Exact: C&L*	Huang
1	10	17·8599	17·9154	17·9154	17·9249	17·9156
	15	17·8599	17·9156	17·9156		
	25	17·8599	17·9156	17·9156		
2	10	34·5268	34·6427	34·6427	34·6752	34·6428
	15	34·5268	34·6428	34·6428		
	25	34·5268	34·6428	34·6428		
3	10	62·5443	62·7886	62·7886	62·8782	62·7886
	15	62·5443	62·7886	62·7886		
	25	62·5443	62·7886	62·7886		
4	10	92·2676	92·6767	92·6767	92·8664	92·6767
	15	92·2676	92·6767	92·6767		
	25	92·2676	92·6767	92·6767		
5	10	133·958	133·613	133·613	/	133·613
	15	133·958	133·613	133·613		
	25	133·958	133·613	133·613		
6	10	174·890	175·602	175·602	/	175·602
	15	174·890	175·602	175·602		
	25	174·890	175·602	175·602		

*Data from Chidamparam and Leissa [25].
"/" indicates that no data is available.

each mode. However, if the desired accuracy was reduced to four significant figures, it only took SAP90 11·15 s to obtain the results by using 128 beam elements, while the present method needed 21·53 s to obtain the solutions with $K = 10$ and $J = 14$ for each of the eight elements through five iterations for each mode. It should be mentioned that all the computation was performed in the PC Pentium DOS environment. For this comparison, one may expect that the present method with some modification [26] can be superior to a finite element solution in the sense of accuracy and computational effort in solving transient problems by using Laplace transform technique because no iteration is involved in the solving process of the proposed method.

5. FREQUENCIES FOR PARABOLIC ARCHES AND ELLIPTIC ARCHES

Having developed a method of analysis with a careful convergence study in the previous sections, an extensive amount of non-dimensional frequency data is presented in this section. The method is demonstrated on parabolic and elliptic arches having uniform rectangular cross-sections with various types of boundary conditions; namely, fixed–fixed, fixed–hinged and hinged–hinged. For parabolic arches, two geometric parameters are varied, which are the ratio of rise, h, to span length, l, and the ratio, $\mu = l/\gamma$ (see Figure 3(a)). For elliptic arches, three geometric parameters are varied, namely, b/a, $\mu = 2a/\gamma$ and the opening angle, θ_0, where a and b represent the lengths of long axis and short axis, respectively (see Figure 3(b)). The representative length of an arch, L, in the solution is set equal to l and $2a$ for parabolic arches and elliptic arches, respectively.

TABLE 3

Convergence of frequency parameters $\omega R^2\sqrt{\rho A/EI}$ *for a fixed–fixed circular arch by using* 16 *elements*

Modes	$(K+1)$ in equations (8)	$(J+1)$ in equations (9) 10	20	40	Exact C&L*	Huang
1	5	17·9299	17·9188	17·9188	17·9249	17·9156
	10	17·9154	17·9156	17·9156		
	15	17·9154	17·9156	17·9156		
2	5	34·6604	34·6457	34·6457	34·6752	34·6428
	10	34·6424	34·6428	34·6428		
	15	34·6424	34·6428	34·6428		
3	5	62·8145	62·7924	62·7924	62·8782	62·7886
	10	62·7877	62·7886	62·7886		
	15	62·7877	62·7886	62·7886		
4	5	92·7056	92·6801	92·6801	92·8664	92·6767
	10	92·6746	92·6767	92·6767		
	15	92·6746	92·6767	92·6767		
5	5	133·640	133·616	133·616	/	133·613
	10	133·609	133·613	133·613		
	15	133·609	133·613	133·613		
6	5	175·629	175·605	175·605	/	175·602
	10	175·596	175·602	175·602		
	15	175·596	175·602	175·602		

*Data from Chidamparam and Leiss [25].
"/" indicates that no data is available.

The general equation for a parabolic arch of span length, l, and rise, h, shown in Figure 3(a), is

$$y = (-4h/l^2)x(x-l). \tag{21}$$

From the definition of radius of curvature and length of curve, one can find that

$$\frac{1}{R} = -\frac{d^2y}{dx^2}\left[1+\left(\frac{dy}{dx}\right)^2\right]^{-3/2} \tag{22a}$$

and

$$\xi = dx/dS = \left(\sqrt{1+(dy/dx)^2}\right)^{-1}. \tag{22b}$$

The general equation for an elliptic arch is

$$x^2/a^2 + y^2/b^2 = 1. \tag{23}$$

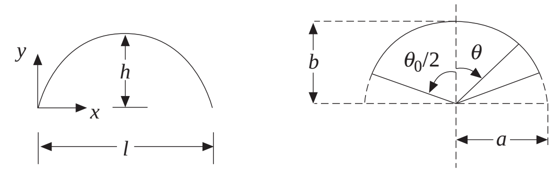

(a) (b)

Figure 3. Arch forms: (a) parabolic; (b) elliptic.

TABLE 4

Frequency parameters $\omega L^2\sqrt{\rho A/EI}$ for fixed–fixed parabolic arches

μ	h/l	Mode 1	2	3	4	5	6
100	0·2	46·0762	87·2729	126·280	155·294	232·386	296·359
	0·4	27·4931	61·3285	104·450	149·958	170·096	215·344
	0·6	16·7617	39·0367	68·0152	101·572	143·181	162·183
	0·8	10·9359	25·7958	45·7441	68·7613	97·6573	131·706
10	0·2	16·2960	21·6086	32·2292	39·4785	55·4119	58·8347
	0·4	14·5769	17·5944	27·6166	29·2302	42·5544	51·3153
	0·6	10·0120	16·4407	21·3980	22·1393	32·3978	41·6115
	0·8	7·12940	14·5055	16·0531	17·6354	25·4230	32·6005

TABLE 5

Frequency parameters $\omega L^2\sqrt{\rho A/EI}$ for fixed–hinged parabolic arches

μ	h/l	Mode 1	2	3	4	5	6
100	0·2	36·6037	78·1589	123·363	140·155	213·421	289·484
	0·4	21·3721	52·4916	93·2011	140·363	166·517	201·226
	0·6	12·8717	33·0188	60·2653	92·7515	132·805	162·163
	0·8	8·34340	21·7199	40·3514	62·5514	90·3211	123·100
10	0·2	14·5577	20·3267	32·0483	38·2834	55·3202	58·0459
	0·4	12·6860	17·3261	27·0204	28·1282	41·9086	51·2479
	0·6	8·50400	16·2720	19·7129	22·0438	31·5855	41·2985
	0·8	5·92400	13·9875	14·9246	17·4059	24·6224	31·9943

It is found that it is very difficult to find the higher order terms in equation (9) even by using Mathematica™. Therefore, polar co-ordinates are used in the formulation instead. Then, by definition,

$$R = (1/ab)\,[a^2\cos^2\theta + b^2\sin^2\theta]^{3/2} \tag{24a}$$

and

$$\mathrm{d}\theta/\mathrm{d}S = [a^2\cos^2\theta + b^2\sin^2\theta]^{-1/2}. \tag{24b}$$

TABLE 6

Frequency parameters $\omega L^2\sqrt{\rho A/EI}$ for hinged–hinged parabolic arches

μ	h/l	Mode 1	2	3	4	5	6
100	0·2	28·7644	68·3075	123·246	124·637	195·015	273·990
	0·4	16·5440	44·3372	82·4977	128·846	165·543	186·739
	0·6	9·88910	27·5004	52·9960	84·0035	122·823	162·033
	0·8	6·38010	17·9707	35·3749	56·3911	83·2737	114·840
10	0·2	13·5699	18·3298	31·9313	36·0778	55·1046	57·7393
	0·4	11·2690	16·6375	26·2117	27·2360	41·1625	51·1814
	0·6	7·18350	15·8479	18·5615	21·4894	30·7286	40·9379
	0·8	4·84950	12·8112	14·7628	16·6995	23·8732	31·3177

To use the formulation of solution given in the earlier section, one needs to set $L = 2a$ and $\eta = \theta_n$, where θ_n is the position angle of nodal point n, and replace x and $\bar{x}$ by θ. In addition, one has to define $\bar{\xi} = L\,\mathrm{d}\theta/\mathrm{d}S$ to replace ξ.

To supplement the available database on parabolic and elliptic arches in the published literature, in Tables 4–9 are listed the non-dimensional frequencies for the first six modes obtained from the present method. The results were obtained by using 16 elements with $J = 29$, and $K = 15$ and $K = 13$ for parabolic arches and elliptic arches, respectively. These results are accurate to six significant figures (from convergence studies not shown here). As one might expect, the natural frequencies increase as the constraints of the boundary conditions increase, from hinged–hinged to hinged–fixed to fixed–fixed if the geometry parameters remain constant. The non-dimensional frequency for each mode decreases as the ratio, μ, decreases, because the ratio, L/γ, is involved in the non-dimensional frequency. Otherwise, from the physical senses, an arch should become more flexible as the ratio, μ, increases, so that the natural frequencies should decrease.

From the results for parabolic arches given in Tables 4–6, the non-dimensional frequencies increase as the ratio of h to l increases, with some exceptions, such as the results for the fourth mode of the hinged–hinged and fixed–hinged arches with $\mu = 100$. For a comprehensive study on the trend of frequency versus h/l for the first three modes of parabolic arches, one should refer to the paper by Lee and Wilson [17].

The results for elliptic arches listed in Tables 7–9 show the decrease of non-dimensional frequency for each mode with the increase of opening angle, θ_0, if other geometry parameters remain constant. This phenomenon makes sense because an arch with a large opening angle is more flexible than one with a small opening angle. The trend for the non-dimensional frequency versus b/a is not clear, and depends on which opening angle, mode, or μ is under consideration. Suzuki and Takahashi [20] gave a comprehensive study

TABLE 7
Frequency parameters $\omega L^2\sqrt{\rho A/EI}$ for fixed–fixed elliptic arches

μ	b/a	θ_0 (degrees)	Mode 1	2	3	4	5	6
100	0·2	60	93·1679	228·641	428·962	625·621	674·906	949·693
		120	49·0833	77·8741	154·973	241·783	357·489	363·472
		180	43·9775	53·8656	122·959	162·311	262·880	272·963
	0·5	60	120·446	221·794	421·938	613·104	673·786	932·173
		120	67·5534	84·2185	160·647	212·414	327·516	358·960
		180	35·9884	50·5204	110·291	136·020	223·450	230·171
	0·8	60	155·586	210·235	409·609	593·964	667·176	902·109
		120	54·4974	92·2983	173·668	181·387	286·121	338·904
		180	22·8741	43·5458	83·1160	121·062	179·076	198·628
10	0·2	60	33·3320	60·9326	64·2812	89·8196	100·394	125·501
		120	17·2305	32·0771	37·5111	53·5737	67·9692	71·8998
		180	14·1519	24·2982	31·6841	43·8130	57·2407	60·6488
	0·5	60	33·8384	57·7223	65·8188	89·7197	98·5407	124·644
		120	18·3746	27·3985	38·4844	49·7225	65·9588	69·0161
		180	14·9332	17·2183	30·1474	36·4781	49·8160	52·6507
	0·8	60	34·6318	54·2016	66·4456	89·4715	95·4355	123·144
		120	19·4572	23·0279	37·4793	44·5055	61·4449	65·0541
		180	12·5152	15·1817	27·0431	29·3985	42·1760	44·3708

TABLE 8

Frequency parameters $\omega L^2\sqrt{\rho A/EI}$ for fixed–hinged elliptic arches

			Mode					
μ	b/a	θ_0 (degrees)	1	2	3	4	5	6
100	0·2	60	70·5699	189·095	379·686	611·629	634·650	892·968
		120	47·9755	63·3659	136·505	218·250	330·331	363·399
		180	38·5975	49·3955	121·096	141·943	241·799	266·071
	0·5	60	107·198	183·223	373·301	590·498	643·236	877·087
		120	54·1738	81·7583	150·869	191·949	302·359	357·014
		180	27·3890	45·5332	97·1136	132·596	208·689	229·826
	0·8	60	147·351	174·642	362·174	565·877	644·833	848·108
		120	42·9955	83·7741	161·672	173·890	263·957	332·063
		180	17·1453	37·9061	74·0436	113·418	167·661	198·436
10	0·2	60	28·8521	60·9305	63·4209	69·3300	100·297	114·572
		120	14·2898	30·9687	37·3644	52·7003	60·8759	71·7809
		180	12·0806	22·8489	31·5688	42·6558	56·2778	59·7551
	0·5	60	29·5129	57·5175	63·5849	71·0279	98·4999	113·164
		120	16·1081	26·1029	38·3942	48·5721	60·6651	68·2841
		180	13·8307	15·8040	30·1458	34·8214	48·9731	52·5012
	0·8	60	30·5501	53·6147	62·2054	72·5597	95·4317	111·022
		120	17·6533	21·7756	37·4263	43·0812	59·9548	62·3981
		180	10·5571	15·1751	27·0204	27·7961	41·3968	43·9261

TABLE 9

Frequency parameters $\omega L^2\sqrt{\rho A/EI}$ for hinged–hinged elliptic arches

			Mode					
μ	b/a	θ_0 (degrees)	1	2	3	4	5	6
100	0·2	60	54·9307	152·053	331·532	561·055	629·857	836·245
		120	47·6857	50·1204	119·854	195·334	303·709	362·503
		180	33·5267	39·5233	121·078	121·465	238·969	244·137
	0·5	60	101·751	146·652	325·821	545·863	634·727	820·923
		120	42·0451	76·0361	146·575	171·293	277·860	350·955
		180	19·9020	38·5404	84·7922	126·747	199·284	227·417
	0·8	60	137·706	148·891	316·002	522·752	636·749	792·914
		120	32·7867	73·8734	146·255	172·843	242·752	319·191
		180	12·0598	32·1018	65·5254	105·119	157·147	197·882
10	0·2	60	25·6337	56·9378	60·9375	65·4179	88·5351	100·977
		120	11·5480	29·3817	37·2397	52·2535	57·2717	68·9501
		180	10·4167	20·9519	31·4877	41·5555	56·1837	56·8498
	0·5	60	26·4744	54·8903	58·8126	68·2068	87·9155	98·8597
		120	14·3964	24·2109	38·3173	47·6956	57·6862	65·7733
		180	13·1908	14·0529	30·1451	32·0610	48·5648	52·0328
	0·8	60	27·8071	51·0292	58·2157	70·2103	86·7567	95·4857
		120	17·0490	19·3719	37·3934	41·7598	57·1597	62·2501
		180	8·67590	15·1569	26·0371	27·0289	40·6919	43·2958

on the relation of frequency parameter to the opening angle for the first two symmetric and antisymmetric modes of elliptic arches.

It is interesting to compare the results for the parabolic arch with $h/l = 0{\cdot}4$ with the results for the elliptic arch with $b/a = 0{\cdot}8$ and $\theta_0 = 180^\circ$ because they have the same span length, rise, and μ but have different shapes. Generally speaking, the results for parabolic arches are larger than those for elliptic arches, with several exceptions for higher modes, and the differences become small for small values of μ.

6. CONCLUDING REMARKS

In this paper, a systematic procedure to obtain a series solution for the free vibration of a uniform arch with variable curvature is presented. The concept of the dynamic stiffness method is introduced into the series solution so that the arch under consideration is decomposed into several subdomains (or elements). In each subdomain, the solutions for displacement components and stress resultants are expressed in the form of polynomials, the coefficients of which are related to each other through recursive equations. As a result, one does not need to expend a lot of effort to find the higher order terms in Taylor expansion series for those geometry functions related to curvature, arc length and their first derivatives (given in equations (9)). In addition, one is always able to obtain convergent results with the required accuracy by increasing the number of elements or the number of polynomial terms in the solution. These have been successfully demonstrated by conducting a convergence study for a uniform circular arch.

The numerical results shown in the paper are the first six modes for parabolic and elliptic arches with various boundary conditions and with different geometry parameters to supplement the available database in the published literature. These data are accurate to six significant figures.

It is because the solution is formulated through a dynamic stiffness matrix that this solution can be easily combined with the dynamic stiffness matrix for straight beam, circular arches or others to solve a more complicated system which includes different types of structural elements. The present procedure can be extended without any difficulty to solve other problems such as in-plane or out-plane vibrations of arches with variable curvature and cross-section. In addition, by introducing the Laplace transform technique into the present solution procedure with some simple modification, one is able to analyze the transient responses of arches with variable curvature and cross-section [26]. To make the proposed procedure more efficient from the point of view of computation, one may want to introduce adaptive refinement techniques available in finite element methods effectively to decompose an arch into elements.

ACKNOWLEDGMENTS

This research was supported by the National Science Council, R.O.C. (NSC 86-2211-E-032-005). Much appreciation is extended to colleagues in the National Center for Research on Earthquake Engineering and in the Department of Civil Engineering in Tamkang University for their kind support which enabled completion of this work.

REFERENCES

1. S. Markus and T. Nanasi 1981 *The Shock and Vibration Digest* **13**(4), 3–14. Vibration of curved beams.

2. P. A. A. LAURA and M. J. MAURIZI 1987 *The Shock and Vibration Digest* **19**(1), 6–9. Recent research on vibrations of arch-type structures.
3. P. CHIDAMPARAM and A. W. LEISSA 1993 *Applied Mechanics Reviews* **46**(9), 467–483. Vibrations of planar curved beams, rings, and arches.
4. J. A. C. BRESSE 1859 *Cours de Mecanique Appliquée*. Paris: Gauthier-Villars; second edition.
5. R. HOPPE 1871 *J. fur Reine und Angewandte Mathematik* (*Crelle's Journal*) **73**, 158–168. Vibrationen eines Rings in seiner Ebene.
6. A. E. H. LOVE 1927 *Treatise on the Mathematical Theory of Elasticity*. Cambridge University Press; fourth edition.
7. K. FEDERHOFER 1933 *Ingenieur Archiv* **4**, 110–120. Biegungsschwingungen eines Kreisringes bei konstantem aussen- oder Innendrucke.
8. L. L. PHILIPSON 1956 *Journal of Applied Mechanics* **23**, 364–366. On the role of extension in the flexural vibrations of rings.
9. A. S. VELETSOS, W. J. AUSTIN, C. A. L. PEREIRA and S.-J. WUNG 1972 *Journal of the Engineering Mechanics Division*, *Proceedings of the American Society of Civil Engineers* **98**(EM2), 311–329. Free in-plane vibration of circular arches.
10. J. HENRYCH 1981 *The Dynamics of Arches and Frames*. New York: Elsevier Science.
11. P. CHIDAMPARAM and A. W. LEISSA 1995 (to appear) *Journal of Applied Mechanics*. Equations governing the in-plane free vibrations and stability of statically loaded curved beams of arbitrary curvature.
12. E. VOLTERRA and D. MORELL 1961 *Journal of the Acoustical Society of America* **33**, 1787–1790. Lowest natural frequencies of elastic hinged arcs.
13. E. ROMANELLI and P. A. A. LAURA 1972 *Journal of Sound and Vibration* **24**, 17–22. Fundamental frequencies of non-circular, elastic, hinged arcs.
14. T. M. WANG 1972 *Journal of the Structure Division*, *Proceedings of the American Society of Civil Engineers* **98**(ST1), 407–411. Lowest natural frequency of clamped parabolic arcs.
15. T. M. WANG and J. A. MOORE 1973 *Journal of Sound and Vibration* **30**, 1–7. Lowest natural extensional frequency of clamped elliptic arcs.
16. T. M. WANG 1975 *Journal of Sound and Vibration* **41**, 247–251. Effect of variable curvature on fundamental frequency of clamped parabolic arcs.
17. B. K. LEE and J. F. WILSON 1989 *Journal of Sound and Vibration* **136**, 75–89. Free vibrations of arches with variable curvature.
18. S. TAKAHASHI, K. SUZUKI, K. FUKAZAWA and K. NAKAMACHI 1977 *Bulletin of the Japan Society of Mechanical Engineers* **20**(148), 1236–1243. In-plane vibrations of elliptic arc bar and sinus curve bar.
19. K. SUZUKI, S. TAKAHASHI and H. ISHIYAMA 1978 *Bulletin of the Japan Society of Mechanical Engineers* **21**(154), 618–627. In-plane vibrations of curved bars.
20. K. SUZUKI and S. TAKAHASHI 1979 *Bulletin of the Japan Society of Mechanical Engineers* **22**(171), 1284–1292. In-plane vibrations of curved bars considering shear deformation and rotary inertia.
21. A. Y. T. LEUNG and W. E. ZHOU 1995 *Journal of Sound and Vibration* **181**, 447–456. Dynamic stiffness analysis of non-uniform Timoshenko beams.
22. E. T. WHITTAKER and G. N. WATSON 1965 *A Course of Modern Analysis*. Cambridge: Cambridge University Press; fourth edition.
23. B. LEAVENWORTH 1960 *Communications of the ACM* **3**, 602. Algorithm 25: real zeros of an arbitrary function.
24. T. M. WANG and M. P. GUILBERT 1981 *International Journal of Solids and Structures* **17**, 281–289. Effects of rotary inertia and shear on natural frequencies of continuous circular curved beams.
25. P. CHIDAMPARAM and A. W. LEISSA 1995 *Journal of Sound and Vibration* **183**, 779–795. Influence of centerline extensibility on the in-plane free vibrations of loaded circular arches.
26. Y. P. TSENG, C. S. HUANG and C. J. LIN 1996 (submitted to) *Journal of the Engineering Mechanics Division*, *Proceedings of the American Society of Civil Engineers*. In-plane transient responses of an arch with variable curvature.